Three-Dimensional Stereotactic Surface Projection Analysis of Macaque Brain PET: Development and Initial Applications

Donna J. Cross, Satoshi Minoshima, Shintaro Nishimura, Akihiro Noda, Hideo Tsukada, and David E. Kuhl

Department of Internal Medicine (Nuclear Medicine) and Neuroscience Graduate Program, University of Michigan Medical School, Ann Arbor, Michigan; Medical and Pharmacological Research Center Foundation, Hakui City; and Central Research Laboratory, Hamamatsu Photonics K.K., Hamamatsu, Japan

To characterize better the local brain functions of conscious rhesus macaques, we developed automated image analysis techniques for monkey PET images, examined the cerebral glucose metabolism of monkeys, and compared it with that of humans. **Methods:** Glucose metabolic PET images from 11 monkeys were obtained using a high-resolution animal PET scanner after intravenous administration of FDG. T1-weighted MR images were obtained from 6 of the monkeys. Referencing a bicommissural stereotactic macaque brain atlas, we created a PET brain template using coregistered MR images. Each individual PET image set was transformed to the PET template through an automated affine transformation, followed by nonlinear warping along the directions of the major neuronal fiber bundles in the brain. For minimization of residual anatomic variability, metabolic activities were extracted using 3-dimensional stereotactic surface projections. The effects of anatomic standardization were evaluated using MR images. Patterns of cerebral glucose metabolism of young versus aged monkeys were examined. The metabolic activities of aged monkeys were compared with those of elderly healthy human volunteers that had been analyzed similarly. **Results:** Anatomic standardization reduced individuals' anatomic variability as evidenced by a reduction in the number of MR pixels with higher SDs calculated across monkeys. Coefficient-of-variation maps of conscious monkeys revealed that the greatest metabolic variances were near the central sulci and occipital cortices. Age-associated glucose metabolic reductions were most pronounced in the occipital lobe, caudate nucleus, and temporal lobe. Compared with human brains, the monkey frontal lobe and posterior cingulate gyrus had significantly less metabolic activity and the supramarginal gyrus and vermis had significantly more metabolic activity. **Conclusion:** The proposed method permits pixel-by-pixel characterization of the metabolic activities of rhesus macaque brains in the stereotactic coordinate system. Greater metabolic variances in the central sulcus region and occipital lobe suggest potential difficulties in controlling sensory input and motor output or planning in conscious monkey experiments. The analyses revealed age-related metabolic reductions in monkeys and marked differences in metabolic patterns between aged monkey brains and aged human brains. The proposed brain-mapping technique enables reproducible and observer-independent analyses and will serve as an important investigative tool for primate brain imaging research.

Key Words: emission CT; rhesus macaque; image analysis; brain; glucose metabolism

J Nucl Med 2000; 41:1879–1887

Recent technical developments in PET have improved the quantitative functional imaging of small animals (*1–3*). The use of PET for animals permits research that cannot be done easily with humans and complements human in vivo imaging experiments. A major use of animal brain PET imaging is the examination of the in vivo kinetics and distribution of new radiotracers (*4–6*). Other uses include pharmacologic interventions to investigate neurochemical changes in the brain (*7*), human disease models (*8–10*), and brain activation studies in conscious monkeys (*11,12*).

Although scanner technology has advanced, image analysis techniques for animal PET remain limited. Most investigations rely on the use of region-of-interest (ROI) approaches. These techniques have several disadvantages. The analysis does not include the entire brain, the density of the data sampling can be biased regionally, reproducibility and consistency among different investigators are limited because of observer dependency, and interinstitutional comparisons are less reliable because of imprecise regional definitions. Better accuracy, reproducibility, and consistency are all essential to data analysis. Minimizing uncertainties in image analysis is critical to maintaining the power of subsequent statistical analyses, particularly with in vivo imaging studies, in which the number of subjects is generally limited. In the analysis of human brain images, attempts have been made to overcome these issues.

The departure from a priori hypothesis-based ROI analyses for human brain images was pioneered by the work of Fox et al. (*13*) and Friston et al. (*14*). These approaches are based on the pixel-by-pixel analysis of functional brain images. First, brain images are standardized anatomically to a common stereotactic coordinate system. Then, functional information can be analyzed statistically on a pixel-by-pixel

Received Aug. 31, 1999; revision accepted Feb. 1, 2000.

For correspondence or reprints contact: Satoshi Minoshima, MD, PhD, Department of Internal Medicine (Nuclear Medicine), University of Michigan, B1G412 University Hospital, Ann Arbor, MI 48109-0028.

basis over the entire brain. This procedure also facilitates the objective definition of ROIs in a common stereotactic system, which reduces observer bias in ROI placement. Friston et al. (*15*) used a mathematic transformation initially applied in 2 dimensions to nonlinearly transform individual PET images to a standard PET template atlas. This method is fully automated and requires only PET images. Minoshima et al. (*16*) proposed the use of cortical and subcortical control points based on the directions of the major neuronal fiber bundles of the brain to deform the individual brain shapes in 3 dimensions to the standard PET template atlas using a spline function. This method has been applied to a variety of human brain image experiments in our laboratory, including activation studies, metabolic image analysis, and neuroreceptor mapping.

The use of a common coordinate system in monkey PET imaging analysis for indirect anatomic localization dates to the mid 1980s. Riche et al. (*17*) reported the use of the orbitomeatal plane as the basis for a quasistereotactic coordinate system of the baboon brain. The orbitomeatal plane was chosen because these external landmarks could easily be identified at the time of scanning, and the subject's head could be aligned accordingly. Cannestra et al. (*18*) developed a 3-dimensional, multimodality brain map of *Macaca nemestrina* based on a coordinate system proposed by Horsley and Clark (*19*). In contrast to these coordinate systems defined by bony landmarks, Martin and Bowden (*20*) proposed the use of the bicommissural line (the line passing through the anterior and posterior commissures) as a basis for stereotaxy. Originally developed by Talairach and Tournoux (*21*), this brain coordinate system has been used widely in analysis of human brain images. The advantage is that brain rather than bony landmarks defines the coordinate system so that individual variation caused by differences in the anatomic relationship between the skull and the brain is eliminated. In addition, the use of bicommissural stereotaxy facilitates more reliable interspecies comparisons (e.g., human versus monkey) of functional and anatomic organization. Bicommissural stereotaxy was also validated for baboon basal ganglia (*22*). Zilles et al. (*23*) extended brain mapping of macaques and humans to better characterize the sensorimotor cortex. Compared with the development of human image analysis, however, image analysis techniques for in vivo monkey brain imaging are limited. To our knowledge, no method has been established to analyze nonhuman primate PET brain images on a pixel-by-pixel basis in the bicommissural stereotactic system.

In this article, we present a method of stereotactic pixel-based image analysis for monkey PET images. The advantages of pixel-based analysis of PET images are multifold. The brain is a complex heterogeneous organ, and the extent of regional metabolic activity, neurochemical distribution, and disease propagation provides significant insight into the mechanisms of these processes. Pixel-by-pixel analysis of functional brain imaging elucidates the extent and magnitude of these processes. Although investigators most often have a priori regional hypotheses, the precise placement of regions of interest to detect relatively small functional changes in a specific brain structure is not always possible even with anatomic side information. The inclusion of the entire brain also eliminates regional selection bias and can elucidate functional changes at multiple sites that are intercorrelated within the brain through direct and indirect neuronal connections. The techniques were developed initially for human PET image analysis (*16*,*24*) and were adapted for the macaque brain in this study. We showed their feasibility in 3 initial applications. First, we analyzed regional cerebral metabolic variances of individual conscious monkeys. Second, we examined the patterns of glucose metabolic reductions between aged monkeys. Finally, we compared the resting cerebral metabolic patterns between aged monkeys and aged healthy humans.

MATERIALS AND METHODS

Subjects

The subjects were 11 unanesthetized male rhesus macaques (*Macaca mulatta*) (mean age ± SD, 13 ± 8 y). The method was developed using a subset of 6 monkeys from which both PET and MR images were obtained. In addition, we compared the overall pattern of the glucose metabolism of a subset of 6 younger monkeys (estimated mean age, 6.2 ± 2 y) to that of 5 older monkeys (estimated mean age, 21 ± 3 y). This aged monkey group was also compared with 5 healthy men (mean age, 70 ± 4 y). The research protocol for the rhesus macaque study was approved by the Central Research Laboratory, Hamamatsu Photonics K.K., Hamamatsu, Japan. The PET imaging protocol for humans was approved by the Institutional Review Board for Human Subject Research at the University of Michigan Medical School, Ann Arbor, MI. Written consent was obtained from each man before the study.

PET and MRI

The monkeys had a surgically implanted acrylic skull plate, which was fastened to a head holder by fixation bars to maintain proper orientation during scanning. The animals were accustomed to the head holder and scanning protocol before the experiment and remained calm throughout the imaging procedure. The animal PET images were obtained at the Central Research Laboratory, Hamamatsu Photonics K.K., using a high-resolution animal PET scanner (SHR-7700; Hamamatsu Photonics K.K.), which has an intrinsic in-plane resolution of 2.6 mm full width at half maximum (FWHM) and collects 31 planes with a 3.6-mm slice separation (*25*). Glucose metabolic PET images were obtained after an intravenous injection of approximately 424 MBq (11.5 mCi) FDG. The FDG injection by automated syringe pump and PET scanning were initiated simultaneously. Serial arterial sampling was performed through a small catheter placed in the femoral artery. Images were reconstructed by a filtered backprojection method with a Hanning filter, resulting in an in-plane reconstructed resolution of 4.5 mm. Tissue attenuation was corrected by an initial transmission scan. Quantitative FDG images were calculated using the image frames from 40 to 60 min after tracer injection based on an autoradiographic method (*26*). T1-weighted MR images were obtained from a subset of 6 monkeys on an MRT-50A/II scanner (Toshiba, Tokyo, Japan) with a magnetic field strength of 0.5 T. The

image matrix consisted of 256 × 256 pixels for 29 slices, with a 3-mm slice separation. The repetition time was 50 ms, and the echo time was 14 ms. Before the analysis, PET and MR images from the same subjects were coregistered into the same orientation using an automated program based on mutual information (*27*).

Glucose metabolic PET images of the men were obtained in a 2-dimensional data acquisition mode using an ECAT EXACT (model 921) scanner (Siemens/CTI Inc., Knoxville, TN), which collects 47 slices with a 3.375-mm slice separation. At 30 min after intravenous injection of 370 MBq (10 mCi) FDG in a dimly lit room with ambient noise, a PET image set was obtained over 30 min. Tomographic images were reconstructed by a filtered backprojection method using a Shepp filter with a cutoff frequency of 0.45 cycles per projection element and standard ellipse-fitting attenuation correction, resulting in a reconstructed resolution of approximately 8 mm FWHM.

Image Analysis

Stereotactic Anatomic Standardization and 3-Dimensional SSP. The proposed method for pixel-by-pixel analysis of the brain images of rhesus macaques consists of anatomic standardization of individual monkey PET images into a common stereotactic coordinate system and 3-dimensional stereotactic surface projections (SSP). The combination of these 2 techniques facilitates the statistical comparison of images within groups as well as between groups. The proposed methods are fully automated and require only PET images that have the anatomic features of gray matter (such as glucose metabolic or perfusion images). For stereotactic anatomic standardization, the algorithm realigns an individual brain image and then performs linear size correction in 3 dimensions. In this step, the algorithm performs an iterative search for 9 affine transformation parameters that give the best spatial matching between the individual image set and a standard atlas template using mutual information (*16*) as a cost function. Once images are transformed to standard stereotactic coordinates, regional anatomic differences between the individual brain and the atlas template are minimized by a thin-plate spline deformation (*28*). The program uses multiple control points and corresponding center points predefined according to major fiber bundles of the brain (*16*). After stereotactic anatomic standardization, gray matter activities are extracted using 3-dimensional SSP on a pixel-by-pixel basis (*24*). The extracted data can be analyzed statistically across subjects.

PET Atlas Template and Predefined Control Points. Automated anatomic standardization requires a digital brain template that is matched anatomically with a standard atlas brain. To develop the anatomic standardization technique for monkey PET, we created a PET template of the rhesus macaque brain in reference to the bicommissural stereotactic macaque brain atlas published by Martin and Bowden (*20*) at the University of Washington. First, 1 monkey MR image was selected for the preliminary template, in which the major cortical and subcortical margins had less than a 3-mm difference from those of the University of Washington atlas after manual realignment to the stereotactic coordinate system and linear scaling in 3 dimensions. A coregistered PET image from the same monkey was transformed to the stereotactic coordinate system using the exact parameters defined in the MR transformation. A symmetric brain image was created by transposing the right hemisphere to the left and was used as the preliminary PET template.

For regional anatomic standardization, cortical and subcortical control points (n = 166), along with center points (n = 50), were predefined for each hemisphere according to the directions of the major neuronal fiber bundles within the brain (*29*). The center points were primarily predefined near the origins of fiber bundles such as the corpus callosum and the optic radiation (*16*). Additional points were predefined in the lateral ventricle for adjustment of the cingulate cortex and caudate nucleus (Table 1). Each center point corresponded to several control points in the same cortical area.

Using the preliminary template with its predefined control and center points, PET images from an additional 5 monkeys were transformed to the stereotactic coordinate system, and the individual regional anatomic variations were minimized by an automated algorithm developed previously for human brain image analysis (*16*). Powell's multidimensional search was used by the algorithm to perform an iterative 9-parameter affine transformation to match spatially the individual PET image to the template using mutual information as a cost function (*30*). Then, for each predefined control point, the nonlinear warping algorithm calculated a profile activity curve between the control point and its corresponding center point on both the PET template and the individual image. An iterative search routine found the best match between the template profile and the individual profile by scaling that used mutual information (*27*) as a cost function. The algorithm then matched spatially the control point on the individual brain to the template control point. The individual brain is warped to the template brain by fitting the estimated control points to predetermined template control points using a thin-plate spline algorithm (*28*). Images from 5 monkeys were standardized anatomically in this manner and averaged across subjects to form a new intermediate template. All 6 monkey brains were then restandardized using this intermediate template. The final template was then created from an average of the 6 transformed images after this third iteration. The high FDG uptake from eye muscle activity was erased before the final summation.

Three-Dimensional SSP Data Extraction Method for Monkey PET. Three-dimensional SSP is an analysis method to extract metabolic activity from cortical gray matter (*24*). By extracting the peak activity for each corresponding area of cortex and assigning it to a surface pixel, the algorithm also can compensate for individuals' differences in cortical thickness and gyri depth in the standard

TABLE 1
Stretching Centers and Surface Landmarks for Nonlinear Warping

Centers	n*	Corresponding surface landmarks	n†
Corpus callosum	6	Frontal, parietal, occipital lobes	40
Optic radiation	1	Occipital lobe, visual cortex	14
Inferior longitudinal fasciculus	3	Temporal lobe	7
Uncinate fasciculus	1	Anterior temporal lobe	13
Middle cerebellar peduncle	1	Cerebellum	7
Lateral ventricle	10	Caudate‡, anterior, posterior cingulate	10
Third ventricle	2	Thalamus‡	2

*Number of predefined centers in each hemisphere. Each center point has several corresponding landmarks in same cortical regions.

†Number of predefined landmarks in each hemisphere.

‡Landmarks were placed in anterior and posterior limbs of internal capsule.

stereotactic system, an ability that is advantageous in intergroup comparisons. This technique has been developed and used in human PET extensively (*31–33*).

Three-dimensional SSP analysis requires a set of predefined surface pixels covering all cortical gray matter structures and a corresponding vector at each surface pixel that is perpendicular to the cortical surface (*24*). To define the set of surface pixels specific to rhesus macaque brain, the coregistered MR images from the 6 monkeys were standardized into the stereotactic system using the estimated transformation parameters. After the removal of nonbrain structures, these images were averaged across subjects. A threshold that defined brain and nonbrain pixels was applied to the summed image set, converting it to a binary image. Pixels covering the lateral and medial surfaces of the brain were defined in the stereotactic coordinate system to delineate the brain surfaces. The moment of a spheric volume centered on each surface pixel was calculated on the binary image, which defined the direction of the vector as perpendicular to the surface of the brain.

In the actual application of 3-dimensional SSP monkey PET analysis, the algorithm searches in 3 dimensions for peak gray matter activity at each predefined surface pixel along the corresponding vector to a 3-mm depth and then projects this peak value back to the surface pixel. In this manner, gray matter activities are extracted to a standard surface format and can be analyzed statistically on a pixel-by-pixel basis.

Validation and Initial Applications

Effects of Anatomic Standardization. The basic performance of the algorithms has been evaluated previously for the human brain (*16*). We validated the effects of anatomic standardization on the matching of gray matter structures using structural information obtained from MR images. PET images of 6 rhesus macaques with corresponding MR images were standardized anatomically using the final template and algorithms. Estimated transformation parameters, including affine transformation parameters and control points, were then applied to each coregistered MR image. Nonbrain structures were removed, and the pixel intensities of each standardized image were normalized to the global intensity. After smoothing with a 3-dimensional gaussian filter (4 mm FWHM), the normalized images were averaged across subjects, and the SDs for pixel intensity were calculated on a pixel-by-pixel basis. For validation, 3 types of SD image sets were created. The first image set was created after stereotactic reorientation alone without linear size correction or nonlinear warping. A second set of images was created after stereotactic reorientation and linear size correction but before nonlinear warping. The third image set was created after consecutive application of reorientation, linear size correction, and nonlinear warping algorithms. We examined the improvement of structural matching by these 3 approaches using both SD maps and pixel histograms. The histograms of pixel SDs were calculated within the approximate brain contour (pixel intensity greater than 1% of the global intensity). Structural mismatches (gray matter, white matter, and cerebrospinal fluid) of different pixel intensities were expected to result in greater SDs that diminish progressively as the algorithms for linear size correction and then nonlinear warping are applied.

Metabolic Variances of Aged Conscious Rhesus Monkeys. In addition to the anatomic examination, we investigated the effects of anatomic standardization on regional variance of functional activities. The regional metabolic activity and individual variance in a subset of 5 aged conscious monkeys was examined using stereotactic anatomic standardization and 3-dimensional SSP techniques. PET images were normalized to the global activity before the analysis. The coefficient of variation at each pixel was calculated for the 3-dimensional SSP extracted data across monkeys, and resultant surface maps were displayed in 3 dimensions. Metabolic variances were also examined by ROI analysis. ROIs for major gray matter structures were predefined on the 3-dimensional SSP images in reference to the stereotactic atlas (*20*). The pixel locations of the highest coefficient of variation were expressed using coordinates defined by the reference atlas (*20*).

Metabolic Comparison Between Aged and Young Monkeys. We compared the cerebral glucose metabolic activity of subsets of 5 aged and 6 young rhesus macaques. The individual images from each group were summed on a pixel-by-pixel basis in the 3-dimensional SSP format, and the 2 groups were compared by means of the *t* statistic. A 2-sample *t* test was performed at each pixel, and *t* values were converted to *z* scores using a probability transformation (*34*). Quantitative cerebral metabolic activities of the 2 groups were also assessed by ROI analysis. The regional values were compared using ANOVA with repeated measures and a posthoc 2-sample *t* test between the aged group and the young group.

Comparison with Metabolic Activity of Aged Human Brains. We compared the glucose metabolic activities of 5 aged rhesus macaques with those of 5 aged humans. The human brain PET images were standardized anatomically and processed using 3-dimensional SSP analysis similarly to the monkey PET images but using a digital brain template, control and center points for nonlinear warping, and surface pixels with vectors for 3-dimensional SSP analysis specifically developed for the human brain. To characterize differences in the metabolic patterns between monkeys and humans, we normalized PET pixel values to the global activity before analysis. The individual image sets of each group were averaged in the 3-dimensional SSP format. The normalized regional cerebral glucose metabolism was then compared using ROIs, defined in the 3-dimensional SSP format for comparable structures that were based on the respective stereotactic atlases (*20,21*). The differences were examined for 14 cortical and subcortical regions using ANOVA with repeated measures and a posthoc 2-sample *t* test.

RESULTS

Effects of Anatomic Standardization

When compared with stereotactic reorientation alone, regional mismatches of brain structures on the MR image sets were reduced markedly by linear size correction and reduced further by nonlinear warping (Fig. 1). On the SD image set created after realignment alone, the rim of high SD at the edge of the brain indicated distinct cortical mismatches across subjects. Linear size correction substantially reduced these mismatches, and nonlinear warping resulted in further improvement. The pixel histograms showed that the number of pixels with a high SD decreased substantially after linear size correction was applied, and a further but more modest reduction was seen after nonlinear warping (Fig. 2).

Glucose Metabolic Variance of Aged Conscious Rhesus Macaques

The areas of highest metabolic variance were in the region of the central sulcus and the right occipital lobe (Fig. 3). The

COLOR

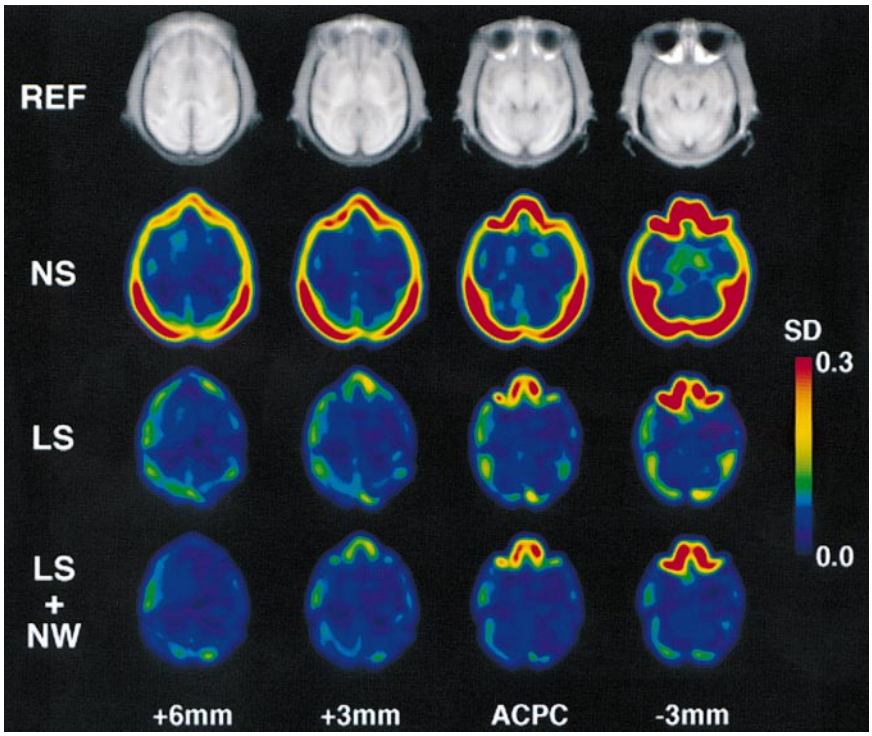

FIGURE 1. Effects of anatomic standardization. Top row represents stereotactic reference MR image set (REF) averaged across 6 monkeys. Second through bottom rows represent SD maps created from MR images (scalp and skull removed) across 6 monkeys with stereotactic realignment alone and no linear scaling (NS), with linear scaling (LS), and with linear scaling and nonlinear warping (LS+NW), respectively. Millimetric scales represent slice levels from anteroposterior commissures (ACPC) in stereotactic space. Areas of higher SDs indicate greater anatomic mismatches. Dramatic reduction of mismatches is seen from NS to LS, and further improvement is seen from LS to LS+NW.

mean coefficient of variation (COV) in these areas was relatively high (right central sulcus, 26%; left central sulcus, 23%; right occipital lobe, 22%) compared with other structures such as the lateral frontal (right, 14%; left, 17%) and lateral parietal (right, 15%; left, 14%) association cortices. However, with this limited sample size, the difference between the highest COV in the right central sulcus and the lowest COV in the right frontal or left parietal association cortices did not reach statistical significance when tested by a variance ratio test. The highest coefficient of variation in the region of the central sulcus was localized to the stereotactic coordinate of (−6, −6, 18) for the right hemisphere and (9, −7, 19) for the left hemisphere according to the University of Washington atlas (*20*). (In this study, positive x, y, and z coordinates denoted left, anterior, and superior, respectively.)

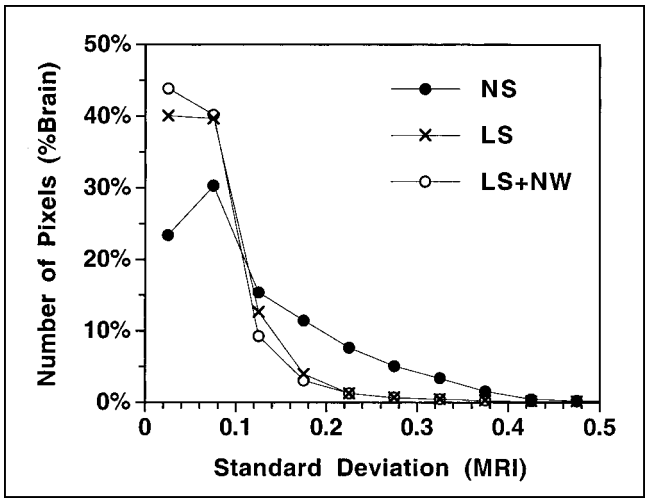

FIGURE 2. Histogram comparing effects of anatomic standardization. Horizontal axis represents SD for each individual pixel for T1-weighted summed MR images across 6 monkeys. Vertical axis represents percentage of brain volume, calculated as number of pixels in each range divided by total number of pixels in brain. Curves illustrate stereotactic realignment alone with no linear scaling (NS), with linear scaling (LS), and with linear scaling and nonlinear warping (LS+NW).

Metabolic Comparison Between Aged and Young Rhesus Macaques

A significant overall metabolic reduction was seen with aging in the brain of rhesus macaques (ANOVA, $F_{1,9} = 6.90$, $P = 0.03$). ROI analysis revealed relatively pronounced metabolic reductions in the occipital lobe, the caudate nucleus, and the temporal lobe (Table 2). The significance of metabolic reductions for most regions, as assessed by a posthoc *t* test, reached a type I error rate of $P < 0.05$, but none of the reductions reached the more stringent criteria of $P < 0.005$ after adjustment for multiple comparisons for this small sample size. Metabolic activities of aged and young rhesus macaques examined by 3-dimensional SSP *z* score showed a similar trend of regional differences between the 2 groups (Fig. 4). Age-associated metabolic reduction was relatively pronounced in the lateral temporo-occipital region compared with the frontal region.

Comparison with Metabolic Activities of Aged Human Brains

The ROI analysis of aged conscious monkeys and aged conscious humans revealed significant differences between the regional metabolic profiles ($F_{1,8} = 6.60$, $P = 0.03$). Compared with aged monkeys, aged humans showed signifi-

COLOR

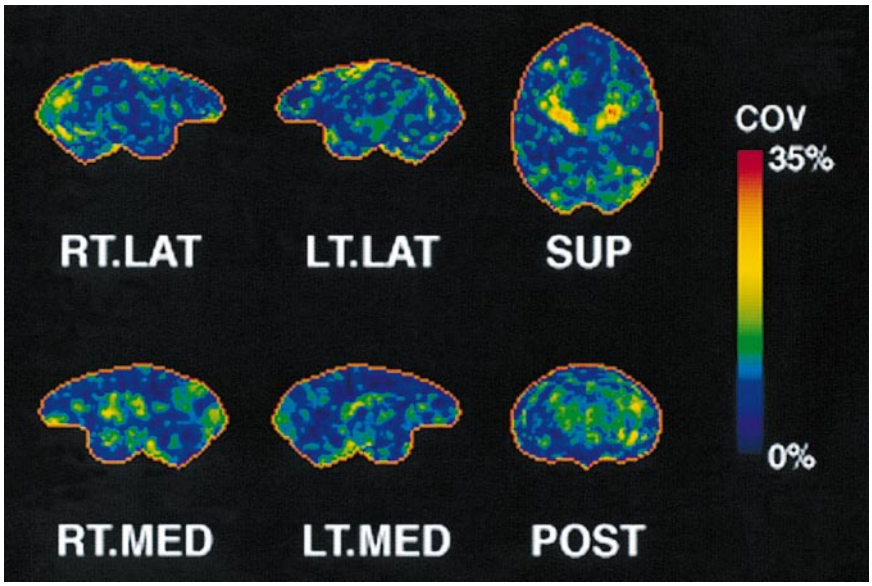

FIGURE 3. Metabolic variances of aged conscious monkey brains. Images were created from calculation of coefficient of variation (COV) at each pixel in 3-dimensional SSP format across 5 monkeys. Top row shows right lateral (RT.LAT), left lateral (LT.LAT), and superior (SUP) aspects of brain, and bottom row represents right medial (RT.MED), left medial (LT.MED), and posterior (POST) aspects of brain. Highest metabolic variance is seen bilaterally in region of central sulcus.

cantly greater metabolic activities in the posterior cingulate and frontal association cortices (Table 3). In contrast, the supramarginal gyrus, cerebellar vermis, and parietal lobe showed significantly lower metabolic activity in human brains compared with monkey brains. Three-dimensional SSP metabolic maps illustrated regional metabolic differences between aged rhesus macaques and aged humans in bicommissural stereotactic space (Fig. 5). The human brains showed relatively greater metabolic activities in the frontal lobe compared with the parietotemporal lobe. In monkeys, the frontal activity was primarily confined to the area of the principal sulcus. In the medial aspect of the brain, the posterior cingulate gyrus had the most intense metabolic activity in resting humans. Such activity was not apparent in monkeys. In contrast, the cerebellar vermis was the area of the highest metabolic activity in conscious aged rhesus macaques.

TABLE 2
Glucose Metabolism in Aged and Young Monkey Brains

	Aged monkey (A)	Young monkey (Y)	A − Y (%)
Cortical structures			
Lateral frontal	25.1 ± 4.3	34.0 ± 7.5	−39*
Lateral parietal	26.8 ± 4.9	37.2 ± 7.8	−39*
Lateral temporal	24.8 ± 3.9	35.2 ± 7.2	−41*
Lateral occipital	25.3 ± 6.3	37.5 ± 8.9	−48*
Cuneus/lingual gyrus	29.5 ± 6.9	40.9 ± 8.4	−39*
Pre-/postcentral gyrus	25.3 ± 5.3	34.4 ± 6.6	−36*
Principle sulcus	27.6 ± 4.9	38.1 ± 7.8	−38*
Supramarginal gyrus	28.5 ± 4.5	39.0 ± 7.5	−37*
Anterior cingulate	27.5 ± 4.5	37.3 ± 8.9	−35
Posterior cingulate	28.1 ± 5.3	38.2 ± 8.6	−36*
Subcortical structures			
Thalamus	29.5 ± 3.2	38.8 ± 7.5	−31*
Caudate	25.0 ± 3.9	37.1 ± 8.1	−43*
Others			
Cerebellum	23.0 ± 4.4	30.8 ± 5.9	−34*
Vermis	31.4 ± 5.9	38.0 ± 5.6	−21
Global average for whole brain	25.1 ± 4.5	34.6 ± 6.9	−38*

*$P < 0.05$.

Regional glucose metabolism (μmol/100 g/min, mean ± SD). A − Y = (A − Y)/A × 100 represents percentage difference between aged monkeys and young monkeys.

DISCUSSION

The proposed methods of anatomic standardization and 3-dimensional SSP data extraction for monkey PET images facilitate better characterization and localization of the cortical functions of rhesus macaques in 3 dimensions as shown in our initial applications. Anatomic standardization minimized structural mismatches across subjects in the standard stereotactic coordinate system. The proposed methods permitted examination in rhesus macaques of the regional metabolic variance between individuals and also of age-related metabolic changes on a pixel-by-pixel basis across subjects. The initial applications also depicted distinct differences between the metabolic profiles of aged conscious monkeys and aged conscious healthy humans.

The effects of nonlinear warping for the monkey brain were less dramatic than in the previous human study (*16*). This difference may be attributed to the relatively uniform shape of the monkey brain across subjects and smaller individual variations in gyri convolution (*29*). A more convoluted human brain has greater need of nonlinear warping to compensate for small individual anatomic variations. Alternatively, although the in-plane resolution of the animal PET scanner (4.5 mm FWHM) is superior to that of a common human scanner (8 mm FWHM), imaging of the relatively small monkey brain may not provide enough structural information to correct small individual anatomic variations. In fact, the ratios of the anteroposterior dimen-

COLOR

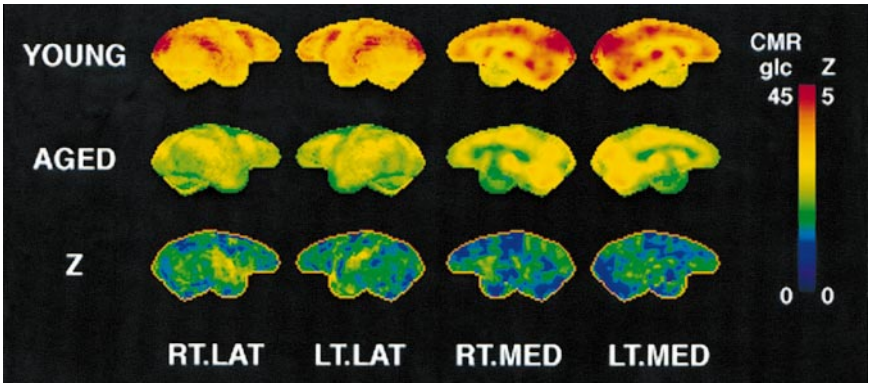

FIGURE 4. Metabolic comparison between aged and young monkeys. Top row represents 3-dimensional SSP of mean pixel values of cerebral metabolic rate of glucose (CMRglc, μmol/100 g/min) averaged across 6 young monkeys. Middle row represents 3-dimensional SSP mean pixel values of CMRglc across 5 aged monkeys. Bottom row represents 3-dimensional SSP of statistical *z* scores (Z) representing significance of regional metabolic reduction of aged group compared with young group. Images are shown as right lateral (RT.LAT), left lateral (LT.LAT), right medial (RT.MED), and left medial (LT.MED) aspects of brain. Higher pixel intensities in first 2 rows represent greater metabolic activities, and higher pixel intensities in bottom *z* score map indicate greater metabolic reductions associated with aging.

sions of the target brain-to-PET scanner resolution are 15 for rhesus macaque imaging (approximately 68:4.5 mm) versus 21 for human imaging (approximately 170:8 mm). The ratios of the dorsoventral dimension–to–plane-to-plane separation are 12 for rhesus macaque imaging (44:3.6 mm) and 33 for human imaging (110:3.375 mm). The ratios on both these axes are far superior for human imaging. A routine use of high-resolution MR imaging for anatomic standardization in monkey experiments may result in an improvement in exchange for additional experimental complexity and a potential new source of errors in PET–MRI registration. The size and location of the regions required by the experimental hypothesis should determine the selection of imaging modalities for anatomic standardization.

TABLE 3
Cerebral Glucose Metabolism in Aged Monkeys and Aged Humans

	Monkey (A)	Human (H)	A − H (%)
Cortical structures			
Lateral parietal	1.07 ± 0.02	1.01 ± 0.03	5*
Lateral temporal	0.99 ± 0.03	0.97 ± 0.02	3
Lateral frontal	1.00 ± 0.03	1.12 ± 0.03	−12†
Lateral occipital	1.00 ± 0.07	1.01 ± 0.04	−1
Cuneus/lingual gyrus	1.17 ± 0.07	1.24 ± 0.07	−6
Pre-/postcentral gyrus	1.00 ± 0.03	0.99 ± 0.04	1
Principle sulcus	1.10 ± 0.04	1.14 ± 0.04	−3
Supramarginal gyrus	1.14 ± 0.04	1.00 ± 0.03	12†
Anterior cingulate	1.10 ± 0.05	1.08 ± 0.03	2
Posterior cingulate	1.12 ± 0.02	1.23 ± 0.04	−10†
Subcortical structures			
Thalamus	1.19 ± 0.08	1.11 ± 0.07	7
Caudate	1.04 ± 0.06	1.08 ± 0.03	−3
Others			
Cerebellum	0.92 ± 0.03	0.99 ± 0.07	−7
Vermis	1.25 ± 0.05	0.92 ± 0.06	27‡

*$P < 0.005$.
†$P < 0.0005$.
‡$P < 0.00005$.
Regional glucose metabolism normalized to global activity (mean ± SD). A − H = (A − H)/A × 100 represents percentage difference between aged monkeys and aged humans. Positive values denote higher metabolism in monkeys.

Our initial application investigating the regional metabolic variance across individual monkeys by coefficient-of-variation images showed relatively higher metabolic variance in the region of the central sulcus. Even though the monkeys were calm from the time of FDG injection to PET imaging, there was a certain amount of motion, planning of movement, and sensory input that was quite variable across subjects. Higher variances in the region of the central sulcus were located in the superior aspect of the brain, suggesting the lower trunk and extremities as a possible source. Higher variability in the sensorimotor activities of conscious monkeys was consistent with the relatively high metabolic variance seen in the occipital lobe. Pixel-by-pixel SD maps of the summed MR images did not show the same degree of variability in these areas, indicating that the variability of the sensorimotor and occipital cortices is functional rather than structural. This finding emphasizes the difficulty in controlling the sensory input or visual imaginary processes in experiments involving conscious monkeys. Despite these limitations, the use of conscious monkeys has a great advantage when studying higher cortical functions such as cortical sensorimotor pathways and cognitive functions using brain activation paradigms (*11*,*12*). The use of conscious monkeys can also eliminate effects from anesthesia in experimental designs. When planning such experiments, one may need to consider greater metabolic variances in these structures for statistical power analysis.

In our comparison between aged and young monkeys, we found an overall quantitative metabolic reduction with age. This reduction was most pronounced in the occipital and temporal cortices. An age-related decline in the cortical

COLOR

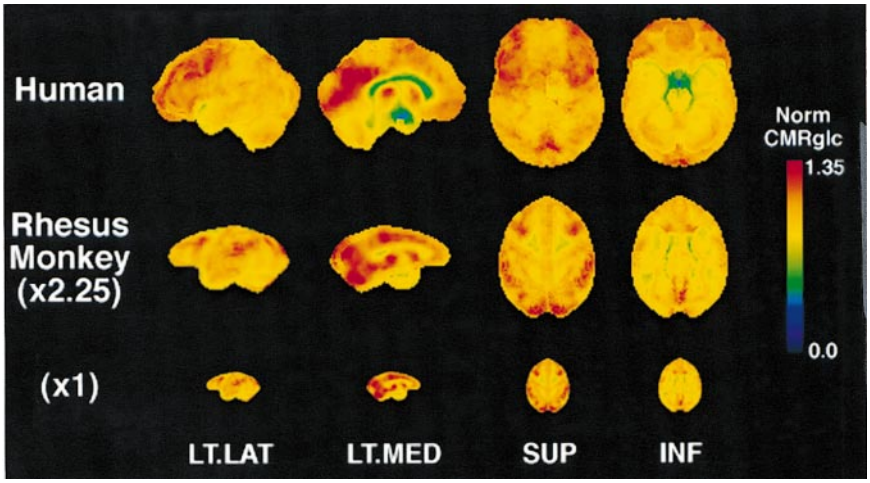

FIGURE 5. Metabolic comparison between aged monkeys and humans. Images represent 3-dimensional SSP of mean pixel values of normalized cerebral metabolic rate of glucose (Norm CMRglc) across 5 aged healthy humans (top row) and 5 aged monkeys (middle row) in left lateral (LT.LAT), left medial (LT.MED), superior (SUP), and inferior (INF) aspects of brain. Bottom row represents actual size of rhesus monkey brain compared with human brain. Images in middle row are magnified (×2.25) for better clarity.

glucose metabolism of conscious rhesus macaques had been reported previously (*35*) and was most significant in the left temporal lobe. Because only minor anatomic asymmetry was indicated in the monkey brain (*36*), we averaged right and left hemispheric values before the ROI analysis to maintain statistical robustness by minimizing the necessity for multiple-comparisons adjustment. Metabolic asymmetry of the monkey brain needs to be addressed with a larger number of subjects in a future experiment.

One of our primary goals for this methodology is to facilitate the application of results from monkey experiments to human research using a common coordinate system. With this in mind, we compared differences in the regional cerebral metabolic patterns between aged monkeys and aged humans. Three-dimensional SSP analysis showed that the human frontal lobe has a greater resting metabolism than does the parietotemporal lobe. In contrast, monkeys have relatively less frontal lobe activity, most of which is centered on the principle sulcus, and have a greater resting activity in the parietotemporal lobe, specifically the supramarginal gyrus. This difference in the overall distributions of resting cortical activity between monkeys and humans may reflect the evolutionary significance of the human frontal lobe (*29*). Human aging is known to preferentially affect the metabolic activity in the frontal lobe (*37*). This reduction in the frontal lobe was not seen in monkeys; rather, a trend of greater reduction was found in occipital and temporal cortices. Analysis of the medial aspect of the human brain shows the highest overall resting activity to be in the posterior cingulate cortex and cinguloparietal transitional area. This area, higher or equal to the metabolic activity of the primary visual cortex in humans but not distinct in monkeys, is the first to show glucose metabolic reduction in early Alzheimer's disease patients compared with healthy humans (*38*). Both visual inspection and ROI analysis revealed that this activity is significantly less in aged monkeys, with the highest resting activity centered on the vermis. These differing patterns of cortical metabolic activities between humans and monkeys suggest potential differences in cortical circuitry and functional development and warrant careful planning in monkey research that will be applied to human physiology and diseases. More nonhuman primate studies with larger sample sizes are needed to fully characterize these differences and to make better comparisons.

Stereotactic anatomic standardization permits the pixel-by-pixel analysis of brain images across subjects (*13*) and facilitates image-based statistical assessment of brain functions (*14*). Initial applications of image-based statistical assessment were aimed at brain activation studies in which individual anatomies were subtracted out in a paired fashion using a common 1-sample statistical test. In this case, residual anatomic variances after stereotactic anatomic standardization reduce the sensitivity in detecting activation. However, when using subtraction techniques across groups (such as using a 2-sample *t* test to compare subjects with disease and healthy subjects), residual anatomic variances can increase false-positive rates and thus reduce the specificity. Three-dimensional SSP further minimizes individual residual anatomic variance, particularly in cortical thickness and depth of gyri, thus reducing false-positive findings (*39*). This method is also less sensitive to the partial-volume effect (*39*), which is still an important issue in small-animal imaging despite the recent advancement in high-resolution scanners. In addition, 3-dimensional SSP analysis permits the assessment of cortical functional patterns in 3 dimensions and can further be supplemented by quantitative ROI analysis defined on 3-dimensional SSP images. Three-dimensional SSP cannot examine deep gray matter such as the putamen and insula. However, these discrete structures can easily be analyzed by a conventional ROI analysis on transaxial slices. Thus, slice-based analysis and 3-dimensional SSP analysis can be used complementarily depending on the experimental hypotheses.

CONCLUSION

The stereotactic image analysis developed in this study permits user-independent and automated statistical analyses of rhesus macaque PET images across subjects in 3 dimensions. The method will be as useful a research tool in

nonhuman primate investigations as it has proven to be in human applications.

ACKNOWLEDGMENTS

The authors thank Michael R. Kilbourn, PhD, and Edward F. Domino, MD, for their valuable comments in the preparation of the manuscript. The authors also thank Douglas M. Bowden, MD, The University of Washington, for his valuable advice about differences in macaque species. This study was supported in part by Department of Energy grant DE-FG02–87-ER60561 and U.S. Public Health Service grant NIH RO1-NS24896.

REFERENCES

1. Moses WW, Virador PRG, Derenzo SE, Huesman RH, Budinger TF. Design of a high-resolution, high-sensitivity PET camera for human brains and small animals. *IEEE Trans Nucl Sci.* 1997;44:1487–1491.
2. Onoe H, Inoue O, Suzuki K, et al. Ketamine increases the striatal N-[^{11}C]methylspiperone binding in vivo: positron emission tomography study using conscious rhesus monkey. *Brain Res.* 1994;663:191–198.
3. Cherry SR, Shao Y, Silverman RW, et al. MicroPET: a high resolution PET scanner for imaging small animals. *IEEE Trans Nucl Sci.* 1997;44:1161–1166.
4. Bergstrom M, Westerberg G, Kihlberg T, Langstrom B. Synthesis of some ^{11}C-labelled MAO-A inhibitors and their in vivo uptake kinetics in rhesus monkey brain. *Nucl Med Biol.* 1997;24:381–388.
5. Kilbourn MR, Snyder SE, Sherman PS, Kuhl DE. In vivo studies of acetylcholinesterase activity using a labeled substrate, N-[^{11}C]methylpiperdin-4-yl propionate ([^{11}C]PMP). *Synapse.* 1996;22:123–131.
6. Mach RH, Ehrenkaufer RL, Greenberg JH, et al. PET imaging studies of dopamine D2 receptors: comparison of [^{18}F]N-methylspiperone and the benzamide analogues [^{18}F]MABN and [^{18}F]MBP in baboon brain. *Synapse.* 1995;19:177–187.
7. Dewey SL, Smith GS, Logan J, et al. Effects of central cholinergic blockade on striatal dopamine release measured with positron emission tomography in normal human subjects. *Proc Natl Acad Sci USA.* 1993;90:11816–11820.
8. Eberling JL, Jagust WJ, Taylor S, et al. A novel MPTP primate model of Parkinson's disease: neurochemical and clinical changes. *Brain Res.* 1998;805:259–262.
9. Melega WP, Raleigh MJ, Stout DB, et al. Longitudinal behavioral and 6-[^{18}F]fluoro-L-DOPA-PET assessment in MPTP-hemiparkinsonian monkeys. *Exp Neurol.* 1996;141:318–329.
10. Volkow ND, Fowler JS, Ding YS, Wang GJ, Gatley SJ. Positron emission tomography radioligands for dopamine transporters and studies in human and nonhuman primates. *Adv Pharmacol.* 1998;42:211–214.
11. Takechi H, Onoe H, Imamura K, et al. Brain activation study by use of positron emission tomography in unanesthetized monkeys. *Neurosci Lett.* 1994;182:279–282.
12. Perlmutter JS, Lich LL, Margenau W, Buchholz S. PET measured evoked cerebral blood flow responses in an awake monkey. *J Cereb Blood Flow Metab.* 1991;11:229–235.
13. Fox PT, Perlmutter JS, Raichle ME. A stereotactic method of anatomical localization for positron emission tomography. *J Comput Assist Tomogr.* 1985;9:141–153.
14. Friston KJ, Passingham RE, Nutt JG, Heather JD, Sawle GV, Frackowiak RS. Localisation in PET images: direct fitting of the intercommissural (AC-PC) line. *J Cereb Blood Flow Metab.* 1989;9:690–695.
15. Friston KJ, Frith CD, Liddle PF, Frackowiak RS. Plastic transformation of PET images. *J Comput Assist Tomogr.* 1991;15:634–639.
16. Minoshima S, Koeppe RA, Frey KA, Kuhl DE. Anatomic standardization: linear scaling and nonlinear warping of functional brain images. *J Nucl Med.* 1994;35:1528–1537.
17. Riche D, Hantraye P, Guibert B, et al. Anatomical atlas of the baboon's brain in the orbito-meatal plane used in experimental positron emission tomography. *Brain Res Bull.* 1988;20:283–301.
18. Cannestra AF, Santori EM, Holmes CJ, Toga AW. A three-dimensional multimodality brain map of the nemestrina monkey. *Brain Res Bull.* 1997;43:141–148.
19. Horsley V, Clark RH. The structure and functions of cerebellum examined by a new method. *Brain.* 1908;31:45–124.
20. Martin RF, Bowden DM. A stereotaxic template atlas of the macaque brain for digital imaging and quantitative neuroanatomy. *Neuroimage.* 1996;4:119–150.
21. Talairach J, Tournoux P. *Co-Planar Stereotaxic Atlas of the Human Brain.* New York, NY: Thieme Medical Publishers; 1988.
22. Black KJ, Gado MH, Videen TO, Perlmutter JS. Baboon basal ganglia stereotaxy using internal MRI landmarks: validation and application to PET imaging. *J Comput Assist Tomogr.* 1997;21:881–886.
23. Zilles K, Schlaug G, Matelli M, et al. Mapping of human and macaque sensorimotor areas by integrating architectonic, transmitter receptor, MRI and PET data. *J Anat.* 1995;187:515–537.
24. Minoshima S, Frey KA, Koeppe RA, Foster NL, Kuhl DE. A diagnostic approach in Alzheimer's disease using three-dimensional stereotactic surface projections of fluorine-18-FDG PET. *J Nucl Med.* 1995;36:1238–1248.
25. Watanabe M, Okada H, Shimizu K, et al. A high resolution animal PET scanner using compact PS-PMT detectors. *IEEE Trans Nucl Sci.* 1997;44:1277–1282.
26. Hutchins GD, Holden JE, Koeppe RA, Halama JR, Gatley SJ, Nickles RJ. Alternative approach to single-scan estimation of cerebral glucose metabolic rate using glucose analogs, with particular application to ischemia. *J Cereb Blood Flow Metab.* 1984;4:35–40.
27. Maes F, Collignon A, Vandermeulen D, Marchal G, Suetens P. Multimodality image registration by maximization of mutual information. *IEEE Trans Med Imaging.* 1997;16:187–198.
28. Bookstein FL. Principal warps: thin-plate splines and the decomposition of deformations. *IEEE Trans Pattern Analysis Machine Intel.* 1989;11:567–585.
29. Ariens Kappers CU, Huber GC, Crosby EC. The comparative anatomy of the nervous system of vertebrates, including man. New York, NY: Hafner Publishing Company; 1960.
30. Press WH, Teukolsky SA, Vetterling WT, Flannery BP. *Numerical Recipes in C.* 2nd ed. New York, NY: Cambridge University Press; 1992:412–420.
31. Albin RL, Minoshima S, D'Amato CJ, Frey KA, Kuhl DE, Sima AA. Fluorodeoxyglucose positron emission tomography in diffuse Lewy body disease. *Neurology.* 1996;47:462–466.
32. Kuhl DE, Minoshima S, Fessler JA, et al. In vivo mapping of cholinergic terminals in normal aging, Alzheimer's disease, and Parkinson's disease. *Ann Neurol.* 1996;40:399–410.
33. Vander Borght T, Minoshima S, Giordani B, et al. Cerebral metabolic differences in Parkinson's and Alzheimer's diseases matched for dementia severity. *J Nucl Med.* 1997;38:797–802.
34. Friston KJ, Frith CD, Liddle PF, Frackowiak RS. Comparing functional (PET) images: the assessment of significant change. *J Cereb Blood Flow Metab.* 1991;11:690–699.
35. Eberling JL, Roberts JA, De Manincor DJ, et al. PET studies of cerebral glucose metabolism in conscious rhesus macaques. *Neurobiol Aging.* 1995;16:825–832.
36. Heilbroner PL, Holloway RL. Anatomical brain asymmetry in monkeys: frontal, temporoparietal, and limbic cortex in *Macaca*. *Am J Phys Anthropol.* 1989;80:203–211.
37. Kuhl DE, Metter EJ, Riege WH, Phelps ME. Effects of human aging on patterns of local cerebral glucose utilization determined by the [^{18}F]fluorodeoxyglucose method. *J Cereb Blood Flow Metab.* 1982;2:163–171.
38. Minoshima S, Giordani B, Berent S, Frey KA, Foster NL, Kuhl DE. Metabolic reduction in the posterior cingulate cortex in very early Alzheimer's disease. *Ann Neurol.* 1997;42:85–94.
39. Minoshima S, Ficaro EP, Frey KA, Koeppe RA, Kuhl DE. Data extraction from brain PET images using three-dimensional stereotactic surface projections. In: Carson RE, Daube-Witherspoon ME, Herscovitch P, eds. *Quantitative Functional Brain Imaging with Positron Emission Tomography.* San Diego, CA: Academic Press; 1998:133–137.